We are IntechOpen, the world's leading publisher of Open Access books
Built by scientists, for scientists

6,900
Open access books available

186,000
International authors and editors

200M
Downloads

154
Countries delivered to

Our authors are among the

TOP 1%
most cited scientists

12.2%
Contributors from top 500 universities

BOOK CITATION INDEX
CLARIVATE ANALYTICS
INDEXED

WEB OF SCIENCE™

Selection of our books indexed in the Book Citation Index
in Web of Science™ Core Collection (BKCI)

Interested in publishing with us?
Contact book.department@intechopen.com

Numbers displayed above are based on latest data collected.
For more information visit www.intechopen.com

Superconducting Properties of Graphene Doped Magnesium Diboride

Xun Xu, Wenxian Li, Xiaolin Wang and Shi-Xue Dou
University of Wollongong/ Institute for Superconducting and Electronic Materials
Australia

1. Introduction

Graphene, carbon in the form of monolayer sheets, has revealed astonishing and unique chemical and physical properties, which have made it an extremely active research topic in both materials science and physics (Novoselov, K. S. et al., 2004). Through chemical and materials integration, graphene is being actively exploited in a range of technological applications (Stankovich, S. et al., 2006). Superconductors can carry electrical current without any energy dissipation. The combination of both graphene and a superconductor into a composite has great potential for electrical devices and large scale applications. MgB_2, a superconductor with a simple composition and two-gap feature has great potential for large current carrying applications, as demonstrated through a series of chemical dopings (Dou, S. X. et al. 2007). In the case of graphene's, the strict two-dimensionality and its high electrical and thermal conductivities, make it an ideal candidate for integrating/doping into MgB_2 in order to improve the superconducting properties.

Substitutional chemistry can modify, in a controlled way, the electronic structures of superconductors and their superconducting properties, such as the transition temperature (T_c), critical current density (J_c), upper critical field (H_{c2}), and irreversibility field (H_{irr}). In particular, carbon containing dopants, including nano-meter sized carbon (nano-C), silicon carbide (SiC), carbon nanotubes (CNTs) and hydrocarbons/carbohydrates are effective means to enhance the J_c- field dependence and H_{c2} (Ma, Y. et al., 2006, Senlowocz, B. J. et al., 2005, Kumakura, H. et al., 2004, Sumption, M. et al., 2005, Dou, S. X. et al., 2003, Kim, J. H. et al., 2006, Wilke, R. H. T. et al., 2008). Upon graphene incorporation into MgB_2 it is expected that H_{c2} and the flux pinning properties should be improved. Recently, high-throughput solution processing of large-scale graphene has been reported by a number of groups (Tung, V. C. et al., 2009, Kim, K. S. et al., 2009, Hernandez, Y. et al., 2008, Li, D. et al., 2008, Li, X. et al., 2008, Choucair, M. et al., 2009).

Based on the works of Choucair et al., sufficient quantities of graphene were obtained for doping the bulk MgB_2 samples via a diffusion process. it was demonstrate that graphene is the most efficient among all the carbon-based dopants used to date, in terms of enhancing the flux pinning behaviour in MgB_2. Very low levels of graphene doping (e,g. 0.9 at%) have been shown to be sufficient to lead to a significant improvement in the critical current density - field performance ($J_c(B)$), with little change in the transition temperature (T_c). At 3.7 at% graphene doping of MgB_2 an optimal enhancement in $J_c(B)$ was reached by a factor of 30 at 5 K and 10 T, compared to the un-doped reference

sample. This improvement is believed to be related to: the single carbon sheet two dimensional (2-D) geometry, the negative thermal expansion coefficient, high electron mobility, low resistivity, high thermal conductivity, and high mechanical strength of graphene. In contrast to many carbon-based dopants, where carbon substitution and hence scattering, is the dominant factor for enhancement of $J_c(B)$, the enhanced flux pinning is largely attributable to strong strain effects induced by the large difference between the negative coefficient of thermal expansion of graphene and the large, anisotropic coefficient of thermal expansion of MgB_2.
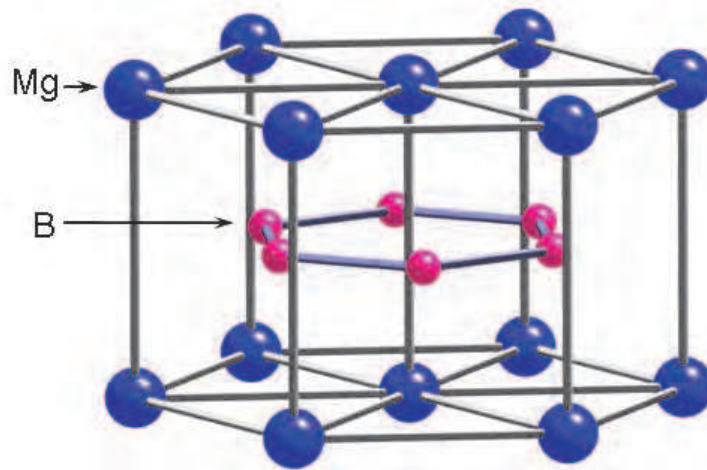

Fig. 1. Crystal structure of MgB_2, a=3.086 Å and c=3.524 Å (Nagamatsu, J. et al., 2001).

The most exciting result is the soften E_{2g} mode in graphene added samples. It is well known that the superconductivity of intermetallic compound MgB_2 is self-optimized both in electronic structure and in phonon dispersion and slim chance is left to improve its superconducting transition temperature, T_c, above ~39.4 K (Nagamatsu, J. et al., 2001). Higher T_c of $Mg^{10}B_2$ and band structure calculation indicate that MgB_2 is a phonon-mediated BCS-Eliashberg superconductor with multiple gaps and strong electron-phonon coupling (EPC). As a two-gap superconductor, MgB_2 shows two qualitatively different Fermi surfaces: σ-band with extremely strong pairing strength and π-band with weak pairing strength. The σ-band contribution is dominant and specifically the contribution from its coupling with the B-B stretch modes with E_{2g} symmetry in boron layer, the only Raman active phonon modes according to first principle calculation (Kunc, K. et al, 2001). the T_c does not show improvements in the alloys due to carbon substitution and impurity scattering, a tensile strain effects assuredly exist in the alloys judging from both the width of superconducting energy gaps and the phonon behaviors.

2. Graphene doped polycrystalline MgB$_2$

MgB_2 is an intermetallic, polycrystalline material that had been known since 1953 and was used in the commercial preparation of elemental boron (B). It was not known to be superconducting until this property was accidentally discovered by Jun Akimitsu and his colleagues (Nagamatsu, J. et al., 2001). MgB_2 consists of alternating layers of boron and magnesium atoms in a hexagonal structure, as shown in Figure 1. It was analyzed that the crystal structure of MgB_2 using by the Rietveld method . It was found that the compound has hexagonal symmetry (Space Group P6/mmm) with the unit cell lattice parameters: a =

0.3086 nm and c = 0.3524 nm. Similar conclusions on the crystal structure were soon made on the basis of studies using high resolution transmission electron microscopy (HRTEM), high resolution powder neutron diffraction and electron energy loss spectroscopy .

Up to now, large number of experimental and theoretical of works has been studied because of its high T_c of 39 K. Beside the high T_c, simple crystal structure, large coherence length, high critical field, transparency of grain boundaries, and low normal state resistivity are a fascinating topic to study for both large scale application and electronic devices. Moreover, the presence of two-gap superconductivity (π and σ band) has been theoretically and experimentally established besides it shows a significant isotope effect like a low temperature superconductor.

2.1 Dual reaction model and C doping effects in MgB$_2$

The "*pure*" MgB$_2$ is not so good for applications due to the poor flux pinning and low J_c, H_{c2} and H_{irr} values. A significant enhancement of critical current density (J_c) in MgB$_2$ can be achieved through chemical doping with various kinds of material. Chemical doping is a simple and readily scalable technique. A significant enhancement of critical current density (J_c) in MgB$_2$ can be achieved through chemical doping with carbon (C) containing composites or compounds, such as SiC, C, B$_4$C, or carbon nanotubes (CNT), hydrocarbon, carbohydrates etc. The C can enter the MgB$_2$ structure by substituting into boron (B) sites, and thus J_c and H_{c2} are significantly enhanced due to the increased impurity scattering in the two-band MgB$_2$.

In 2007, Dou et al has proposed a dual reaction model based on the following factors to explain the mechanism of enhancing the electromagnetic properties due to the SiC and C doping (Dou, S. X. et al. 2007):

- Demonstrated a dual reaction model in which the C substitution due to nano SiC doping and MgB$_2$ formation take place simultaneously at temperatures
- The C substitution and induced highly localised fluctuation in structure and T_c are responsible for the enhancement in J_c, Hirr and Hc$_2$ by SiC doping.
- Disorder created by all means has universal influence on electromagnetic properties of MgB2
- free and reactive C is the key to searching for better do pants
- Fig. 2 shows the effects of sintering temperature on the J_c(H) for different carbon based dopants. The hydrocarbon and SiC doped MgB$_2$ show significant enhancement in J_c for the samples sintered at lower temperature, whereas the carbon and CNT doped MgB$_2$ need to be sintered at higher temperature for high J_c. The low sintering temperature results in small grain size, high concentrations of impurities and defects, and large lattice distortion, which are all responsible for a strong flux pinning force (Soltanian et al., 2005, Yamamoto et al., 2005). Furthermore, the hydrocarbon and SiC can release fresh and active free carbon at very low temperature, which means that the carbon substitution effects take place simultaneously with the MgB$_2$ formation. A high sintering temperature will perfect the crystallization and decrease the flux pinning centers in the MgB$_2$ matrix. That is the reason why high sintering temperature degrades the J_c performance. Although high sintering temperature has the same shortcomings in nanosized carbon and CNT doped MgB$_2$, the carbon substitution effects improve their J_c values. The high sintering temperature is necessary for carbon and CNT doped MgB$_2$ because the carbon and CNT are quite stable at low temperature and the substitution effects are absent if the sintering temperature is not high enough.
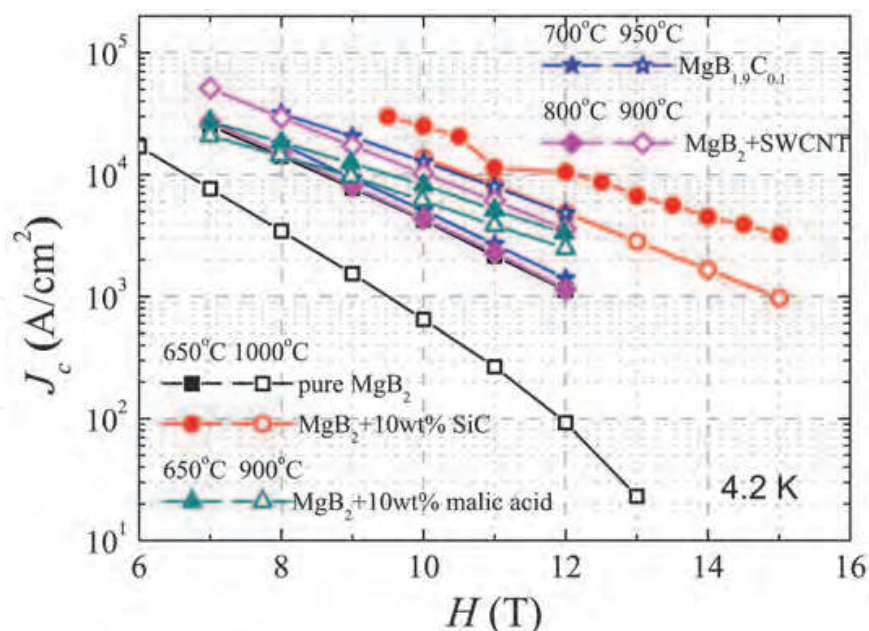
Fig. 2. The critical current density (J_c) at 4.2 K versus magnetic field for wires of pure MgB_2 and MgB_2 doped with C, SiC, SWCNTs, and malic acid that were sintered at different temperatures (Dou et al., 2002; Yeoh et al., 2006; Dou et al., 2007; Kim et al., 2008)

2.2 Gram-scale production of graphene

Graphite is the most common allotrope of carbon. The name isderived from the Greek verb graphein, 'to write', which relates very literally to the compound we now know as graphene, as single sheets of graphene were first isolated by simply tracing a sample of bulk graphite across a substrate in a process known as micromechanical cleavage (Novoselov, K. S. et al., 2004). Further attempts to synthesize isolated graphene have been based on intercalation (Li, X. et al., 2008), sonication in various solvents (Hernandez, Y. et al., 2008) and the chemical reduction of graphite to yield few-layer graphite oxide (Li, D. et al., 2008). Approaches developed for the production of carbon nanotubes have also been explored, but so far they have only been able to produce graphitic film (Dikin, D. A. et al., 2007). However, single- and few-layer graphene sheets have been grown epitaxially by the chemical vapour deposition of hydrocarbons on metal and nonmetal substrates, substrate-free deposition and by thermal decomposition of SiC. Given the lack of a reliable top-down approach for the large-scale production of graphene, attention has turned to bottom-up approaches that might be able to deliver the economies of scale that are found in the chemical and pharmaceutical industries. Choucair et al. have demonstrated that single-layer graphene can be synthesized by low-temperature flash pyrolysis of a solvothermal product of sodium and ethanol, followed by gentle sonication of the nanoporous carbon product (Choucair, M. et al., 2009).

All solvothermal reactions were performed in a Teflon-lined Parr Instrument Company 4749 reactor having a maximum volume of 23 ml. A typical synthesis consists of heating a 1:1 molar ratio of sodium (2 g) and ethanol (5 ml) in a sealed reactor vessel at 220°C for 72 h to yield the solid solvothermal product—the graphene precursor. This material is then rapidly pyrolysed, and the remaining product washed with deionized water (100 ml). The suspended solid is then vacuum filtered and dried in a vacuum oven at 100°C for 24 h. The final yield of graphene is approximately 0.1 g per 1 ml of ethanol—typically yielding ~0.5 g

Fig. 3. Example of the bulk quantity of graphene product. The image consists of approximately 2 g of sample (Choucair, M. et al., 2009).

per solvothermal reaction.The product of this reaction is then washed in water and dried to obtain pure graphene (Fig. 3). Solvothermal reactions have been reported to lead to the production of carbon nanosheets, although such materials do not appear to consist of single sheets having both high degrees of planarityand crystallinity, suggesting an amorphous or disordered graphitic structure (Choucair, M. et al., 2009).

2.3 Graphene doping effects in MgB$_2$

Based on the works of Choucair et al., sufficient quantities of graphene were made available for doping the bulk MgB$_2$ samples. The bulk MgB$_2$ samples were fabricated via a diffusion process. The crystalline boron powder (0.2 to 2.4 µm) 99.999% without and with graphene was prepared by ball milling with toluene medium. Then, the powders were dried in a vacuum oven to evaporate the medium. These powders were mixed and pressed into pellets. The pellets were then put into an iron tube filled with Mg powder (-325mesh 99%). The samples were sintered at 850°C for 10 hrs in a quartz tube; the heating rate was 5°Cmin^{-1} under high purity argon (Ar 99.9%) gas. The phase and crystal structure of all the samples were investigated by X-ray diffraction (XRD). T_c was defined as the onset temperature at which diamagnetic properties were observed. The magnetic J_c was derived from the width of the magnetization loop using Bean's model by a Physical Properties Measurement System (PPMS). Transport measurements for resistivity (ρ) were done using a standard AC four probe method. In addition, $H_{c2}(T)$ and $H_{irr}(T)$ were defined as the fields where the temperature dependent resistance at constant magnetic field R(H_{c2}, T) = 0.9R_{ns} and R(H_{irr}, T) = 0.1R_{ns} with R_{ns} being the normal state resistance near 40 K. The hysteresis loops of the MgB$_2$ sample every 1.5 K in the 17- 35 K range. The symmetric hysteresis loops with respect to the magnetic field indicate the dominance of bulk pinning up to temperatures near T_c.

MgB$_2$/Fe monofilament wires were prepared by an *in situ* reaction process and the powder-in-tube method. Magnesium (99%, 325 mesh), and the different boron powders with the nominal atomic ratio of Mg : B = 1.1 : 2 were mixed through grinding and were put into Fe

tubes with a length of 140 mm, an outer diameter (O.D) of 10 mm, and an inner diameter (I.D) of 8 mm. The packing process was carried out in air. Both ends of the tubes were sealed with aluminum pieces, and then the tubes were drawn to a wire with a diameter of 1.4 mm. Short wire samples (4 cm each) were sealed with Zr foil, then sintered with a heating rate of 5 °C min^{-1} in flowing high purity Ar to 700-800 °C and held at the final temperature for 30 minutes, followed by a furnace cooling to room temperature. The transport current (I_c) at 4.2 K was measured by the standard dc four-probe resistive method with a criterion of 1 μVcm^{-1} in magnetic fields up to 12 T. T_c was determined using the standard ac four-probe method. In addition, $H_{c2}(T)$ and $H_{irr}(T)$ were defined as the fields where the temperature dependent resistance at constant magnetic field $R(H_{c2}, T) = 0.9R_{ns}$ and $R(H_{irr}, T) = 0.1R_{ns}$, respectively, with R_{ns} being the normal state resistance near 40 K.

The common format $Mg(B_{1-x}C_x)_2$ with x=0, 0.037, was used. The composition of graphene doped MgB_2 were 0, 3.7 at%, and as such, the samples are designated as G000, and G037respectively.

2.3.1 XRD analysis for bulk samples

Fig. 4 shows XRD patterns for the pure and graphene doped MgB_2 samples. All the peaks are inherent to MgB_2. No impurity phase was detected in the XRD data, however a slight peak shift to higher angle is noted for the G087 samples. MgO, which is commonly present in most bulk MgB_2 samples is absent in all the samples.

The lattice parameters, a, c, the ratio of a/c, grain size, strain, and full width at half maximum of the representative peak (110) calculated from the XRD patterns are shown in Table 1. Both the a-axis and c-axis parameters vary little with increasing graphene doping level of 3.7%, apart from G087 sample, which shows a notable decrease in the a-axis parameter, suggesting that carbon (C) likely substitutes into the boron (B) sites, leading to a slight drop in T_c (36.7 K) for the G087 sample. it also observed that the full width at half maximum (FWHM) of the (110) peak increases with increasing graphene doping level. Such a peak broadening is caused by both grain size reduction and an increase in lattice strain. The calculated results on grain size and lattice strain from a Williamson-Hall plot (Williamson, G. K., and Hall, W. H., 1953) are given in Table 1. Transition temperatures (T_c) for the graphene doped samples were determined by AC susceptibility measurements. Also, the T_c onset determined from the AC susceptibility measurement is 38.9 K for the un-doped sample, dropping only slightly to 37.7 and 36.7 K for the G037 and G087 samples, respectively.

Sample	Lattice Constants			Grain Size (nm)	Strain (%)	FWHM (110) (°)	T_c (onset) (K)
	a (Å)	c (Å)	c/a				
G000	3.084(1)	3.525(1)	1.143(1)	216(10)	0.1198(188)	0.288	38.9
G037	3.082(1)	3.527(1)	1.144(1)	170(8)	0.1685(250)	0.400	37.7
G087	3.075(1)	3.525(1)	1.146(1)	171(11)	0.1782(330)	0.414	36.7

Table 1. The full width at half maximum (FWHM) of the (110) peak, the lattice parameters, and the transition temperature (T_c) for the MgB_2 samples, made with 0, 3.7, and 8.7 at% graphene doping via a diffusion process (Xu, X. et al., 2010).
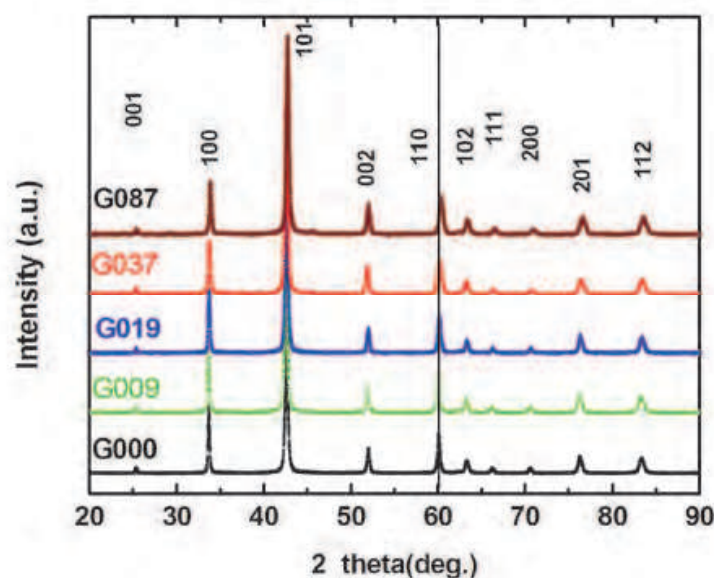
Fig. 4. XRD patterns for graphene doped MgB_2 samples: G000, G009, G019, G037, and G087, showing that all diffraction peaks can be indexed to MgB_2 with undetectable impurity phases.

2.3.2 Critical current density

Graphene is the most efficient among all the carbon-based dopants used to date, in terms of enhancing the flux pinning behaviour in MgB_2. Very low levels of graphene doping (e,g. 0.9 at%) have been shown to be sufficient to lead to a significant improvement in the critical current density - field performance ($J_c(B)$), with little change in the transition temperature (T_c). At 3.7 at% graphene doping of MgB_2 an optimal enhancement in $J_c(B)$ was reached by a factor of 30 at 5 K and 10 T, compared to the un-doped reference sample. In contrast to many carbon-based dopants, where carbon substitution and hence scattering, is the dominant factor for enhancement of $J_c(B)$, the enhanced flux pinning is largely attributable to strong strain effects induced by the large difference between the negative coefficient of thermal expansion of graphene and the large, anisotropic coefficient of thermal expansion of MgB_2.

The common format $Mg(B_{1-x}C_x)_2$ with x=0, 0.037, and 0.087 was used. The composition of graphene doped MgB_2 were 0, 3.7, and 8.7 at%, and as such, the samples are designated as G000, G037, and G087, respectively. Fig.5 shows the magnetic $J_c(B)$ curves at 5 K and 20K for all the samples, which were sintered at 850°C for 10 hours. The $J_c(B)$ values for all the doped samples are higher than the un-doped sample at high fields. The sample G037 gives the highest J_c at high fields: J_c increases by a factor of 30 at 5 K for the field of 10 T, as compared to the un-doped sample, G000. Even though the J_c in the low field regime is depressed, a higher doping level (G087), still results in the rate of J_c dropping much slower than the un-doped sample, clearly indicating strong flux pinning induced by the graphene doping. The most significant effect of graphene doping is the high effectiveness of graphene to improve flux pinning at lower doping levels, which distinguishes graphene from any other C containing dopants, for example, the J_c for G037 reached 20,000 A/cm² at 5 K and 8 T, exceeding or matching the best J_c resulting from dopants such as SiC, CNT, and carbohydrates at their optimal doping level of 10 at%, as well as nano-C at its optimal
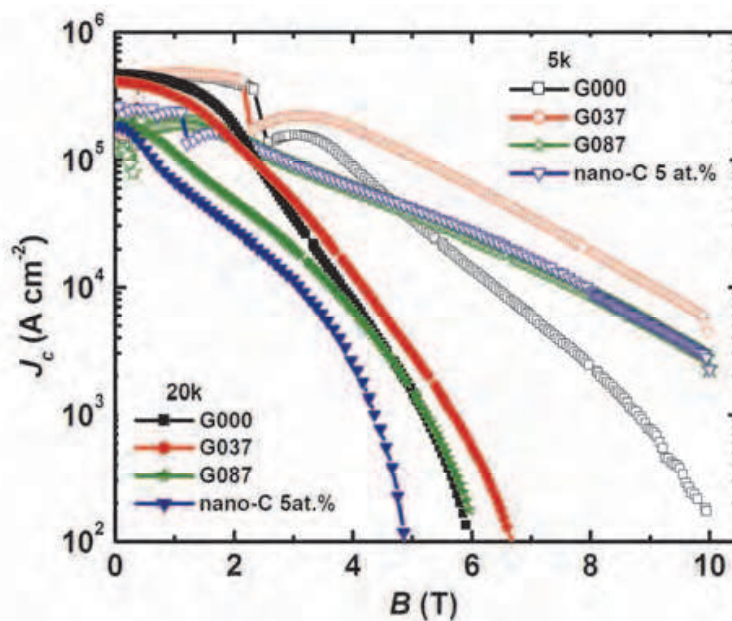
Fig. 5. Magnetic critical current density as a function of magnetic field at 5 K and 20K for with and without graphene doped bulk samples. 5 at% nano-C doped sample for a comparable result at the same sample preparation route (Xu, X. et al., 2010).

doping level of 5-6.4 at.%. In the latter case, the T_c is substantially reduced to temperatures as low as 30 K. Compared to the graphite doped MgB_2 pallets prepared through the ball-milling and HIP the J_c of graphite doped MgB_2 is better than graphene doping at 5 K (Yamamoto et al., 2005), but at 20K, the J_c for graphene doping is much better than graphite. For example, the J_c for the graphene doped MgB_2 at 20 K and 6 T is larger than that for graphite doped MgB_2 by a factor of 50 (Yamamoto et al., 2005). In comparison, low levels of graphene doping have little effect on T_c and cause only a very small increase in impurities, not compromising the significant enhancement in J_c in high fields by the degradation in low-field J_c, which is a common issue for all other C based dopants. In order to see the difference with other C based dopants, the same preparation route was applied to 5 at% nano-C doped sample and the resultant decrease in J_c at 20K can be seen in the figure 5, because the T_c for nano- C doped MgB_2 is only 34K.

The transport current J_{ct}-B performance of the two kinds of the samples sintered at temperatures from 700 °C to 800 °C, denoted by, WG37S7, WG37S8 for 3.7 at% graphene doped and WG0S7, and WG0S8 for undoped wire sample, respectively, is shown in Figure 6. It can be clearly seen that J_{ct} of samples prepared from the doped wire sample showed better performance in the field range of 4 to 15 T. This indicates that the most significant effect of graphene doping is the high effectiveness of graphene to improve flux pinning at lower doping levels. The strong enhancement in the flux pinning may be attributable to a combination of C substitution for B and thermal strain-induced defects. It is very surprised that if compared to the magnetic J_{cm} with the bulk MgB_2 samples via a diffusion process under magnetic fields of 5 to 10 T, the transport J_{ct} increment with the wire MgB_2 via the powder-in-tube (PIT) method is tremendous lower from Fig.6. The transport current capacity is the real useful J_c that flows through the whole of the sample. It can be understand, the difference between J_{cm} and J_{ct} in MgB_2 may be related to features of the microstructure of the superconducting MgB_2 core, such as porosity, agglomeration of
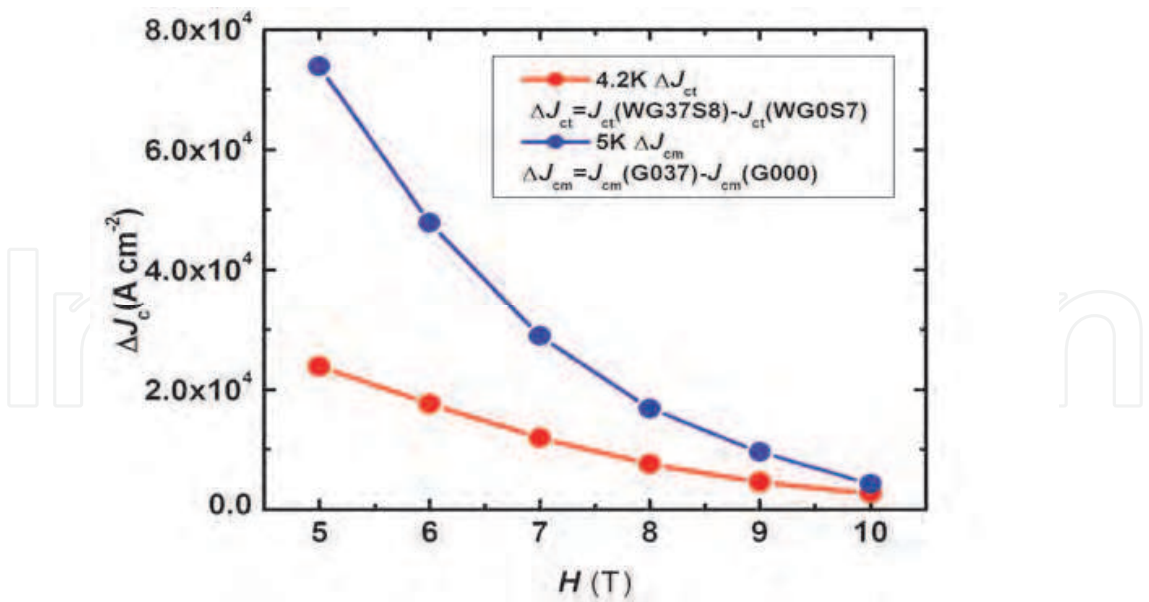
Fig. 6. Compared to the increment of magnetic J_{cm} at 5K and transport J_{ct} at 4.2K

superconducting crystals, and fraction of impurities as the main secondary phase by different fabricated processing (Horvat, J. et al., 2008). It is clearly that the graphene doped bulk sample via the diffusion process had the highest mass density, which improved the most inter-grain connectivity to improve the J_c so much. At the same time, according to the Rowell connectivity analysis, the calculated active cross-sectional area fraction (A_F) represents the connectivity factor between adjacent grains, which is estimated by comparing the measured value with that of a single crystal. (Rowell, J. M., 2003). The A_F for all wire samples via the powder-in-tube (PIT) method is almost half of the bulk sample via diffusion process. With the wire doped samples, the A_F value was increased as the sintering temperature increased. This indicates that additional grain growth occurs due to high temperature sintering. The larger grains are also accompanied by improved density and grain connectivity. So, in order to improve the J_c of the wire sample, the key point is how to improve the inter-grain connectivity.

2.3.3 Flux pinning mechanism

Regarding the flux pinning mechanism, it is established that the core interaction, which stands for the coupling of the locally distorted superconducting properties with the periodic variation of the superconducting order parameter is dominant over the magnetic interaction for MgB₂ due to its large GL coefficient κ (~26 in MgB₂). The core interaction includes two types of mechanism: δT_c and δl pinning. The δT_c pinning refers to the spatial variation of the GL coefficient associated with disorder due to variation in the transition temperature T_c, while δl pinning is associated with the variation in the charge-carrier mean free path l near lattice defects. According to the collective pinning model, the disorder induced spatial fluctuations in the vortex lattice can be clearly divided into different regimes depending on the strength of the applied field: single-vortex, small-bundle, large-bundle, and charge-density-wave (CDW)-type relaxation of the vortex lattice. The crossover field, B_{sb} is defined as a field separating single vortex regime into small bundles of vortices. Below B_{sb}, J_c is almost field independent. The B_{sb} as a function of reduced temperature (t=T/T$_c$) is described by the equation (Qin, M. J. et al, 2002):

$$B_{sb} = B_{sb}(0)\left(\frac{1-t^2}{1+t^2}\right)^{2/3} \tag{1}$$

for δT_c pinning,

$$B_{sb} = B_{sb}(0)\left(\frac{1-t^2}{1+t^2}\right)^2 \tag{2}$$

for δl pinning.

To define the pinning mechanism in our grapheme doped the samples, the crossover field, B_{sb}, as a function of temperature with graphene doped sample (G037) is plotted in Figure 7 as red squares. B_{sb} is defined as a field where J_c drops by 5% only compared to J_c at zero field. It can be seen that the curve for δT_c pinning calculated from q. (1) is in a good agreement with the experimental data, whereas, the curve for δl pinning according to Eq. (2) does not fit to the experimental data. For polycrystalline, thin film, and single crystalline MgB$_2$ samples, it has been found that the dominant pinning mechanism is δT_c pinning, which is related to spatial fluctuation of the transition temperature while most C-doped MgB$_2$ samples displayed δl pinning mechanism (Wang, J. L. et al., 2008) as a result of strong scattering and hence the shortening of the mean free path l owing to the presence of large amount of impurities in the doped samples. This is reflected by the significant increase in the residual resistivity. The local strain was suggested to be one of potential pinning centres.
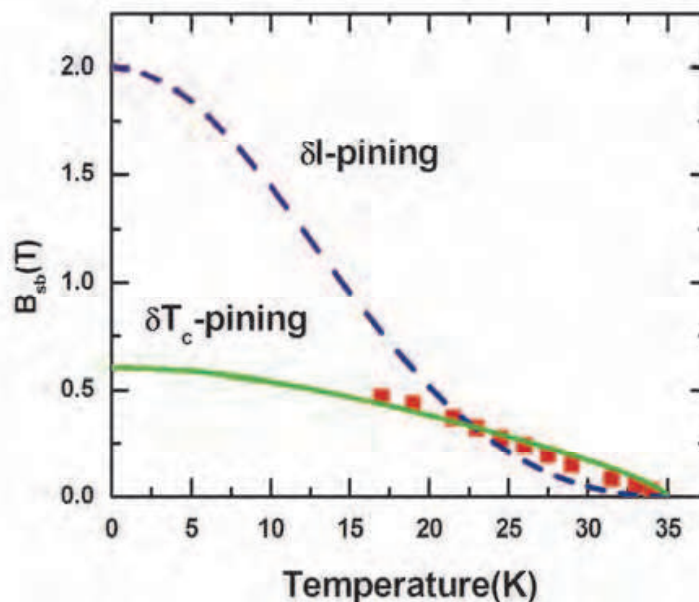

Fig. 7. The crossover field B$_{sb}$ as a function of temperature with graphene doped sample (G037) (Xu, X. et al., 2010)

However, we do not have strong evidence that the dominant pinning in the graphene doped MgB2 is due to the local strain effect alone. In contrast, the graphene doping sets an exceptional example, following the δT_c pinning rather than δl pinning mechanism. This demonstrates the unique feature of the graphene doping. The amorphous phases can also

act pinning centres, which is in favour for δT_c pinning. Although the graphene doped samples have a lot of defects these samples contain low concentration of impurities compared to the samples by other forms of carbon dopants. One of major differences of graphene doping from other dopants is that the samples are relatively pure as evidenced by the low resistivity (20 μΩ cm) in the grapheme doped samples. Normally, the resistivity in carbon doped MgB_2 ranges from 60 μΩ cm to as high as 300 μΩ cm. The high electrical connectivity is beneficial for J_c in low magnetic fields and high field performance; however we can not find any correlation between electrical connectivity with the J_c in the case here. The graphene doped samples have higher resistivity than the un-doped MgB_2 sample (3 μΩ cm), indicating electron scattering caused by graphene doping levels. But, it should be pointed out that the increase in resistivity is much smaller than for any other forms of carbon doped MgB_2, Which is shown in Figure 8.

2.3.3 E_{2g} mode and Raman peak shift

Tensile strain effects on superconducting transition temperature (T_c) was observed in graphene-MgB_2 alloys to pursue high T_c in multi-gap superconductors. The enhancement of energy gap for π-band indicates the weak rescale of density of state on Fermi surface. The E_{2g} mode split into two parts: one dominant soften mode responding to tensile strain and another harden mode responding to carbon substitution effects.
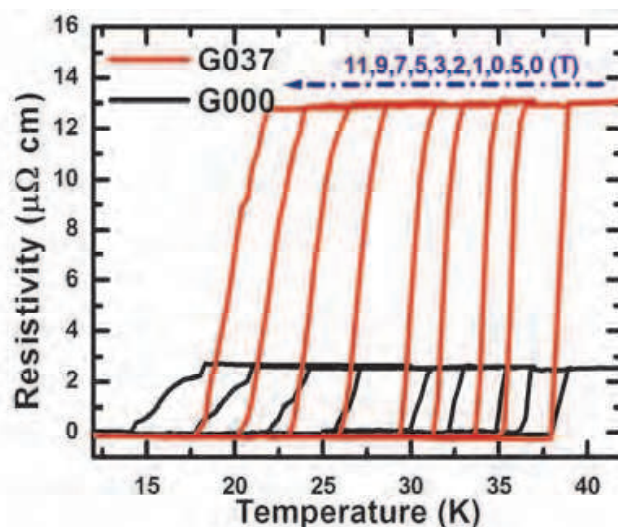

Fig. 8. The temperature dependence of the resistivity (ρ) measured in different fields for doped and undoped samples.

The existence of soften E_{2g} mode in bulk samples suggests that modified graphene-MgB_2 alloys are the potential candidates for the high performance superconducting devices.

To confirm the effect of tensile strain on EPC, Raman scattering was employed for measurement of phonon properties by a confocal laser Raman spectrometer (Renishaw inVia plus) with a 100× microscope. The 514.5 nm line of an Ar+ laser was used for excitation and several spots were selected on the same sample to collect the Raman signals to make sure that the results were credible. Fig. 9(a) shows the typical spectrum of pure MgB_2 consisting of three broad peaks. The most prominent phonon peak located at lower frequency (ω_2: centered at ~600 cm^{-1}) is assigned to the E_{2g} mode. The other two Raman bands (ω_1: centered at 400 cm^{-1} and ω_4: centered at 730 cm^{-1}) have also been observed earlier

in MgB_2 and attributed to phonon density of states (PDOS) due to disorder. The EPC strength in MgB_2 depends greatly on the characteristic of E_{2g} mode, both frequency and FWHM, while the other two modes, especially the ω_4 mode, are responsible for the T_c depression in chemically doped MgB_2 (Kunc, K. et al, 2001). The graphene addition in MgB_2 induces splitting of E_{2g} mode: one soften mode (ω_2) and another harden mode (ω_3), as shown in Fig. 9. ω_2 shifts to low frequency quickly with the graphene addition because of the strong tensile strain. The softness of E_{2g} mode was observed only in MgB_2–SiC thin films due to tensile strain-induced bond-stretching, which resulted in a T_c as high as 41.8 K. Although ω_2 modes are dominant in low graphene content samples, T_c drops slightly. This is in agreement with the energy gap behaviors because of the carbon substitution induced band filling and interband scattering. ω_2 is marginal in G10 and vanishes in G20. ω_3 shifts to high frequency slowly in low graphene content samples because the tensile strain has confined the lattice shrinkage. However, the tensile strain can not counteract the intensive carbon substitution effects when the graphene content is higher than 10 wt% and ω_3 takes the place of ω_2. It should be noted that ω_3 is not as dominant as ω_2 in pure MgB_2 and ω_4 is the strongest peak as in the other carbonaceous chemical doped MgB_2 due to lattice distortion. Furthermore, another peak ω_5 has to be considered in G10 and G20 to fit the spectra reasonably. The Raman spectrum of G20 was separated from the mixed spectra of MgB_2 and MgB_2C_2 based on their different scattering shapes: MgB_2 shows broaden and dispersed waves, while MgB_2C_2 shows sharp peaks (Li, W. X. et al., 2008).

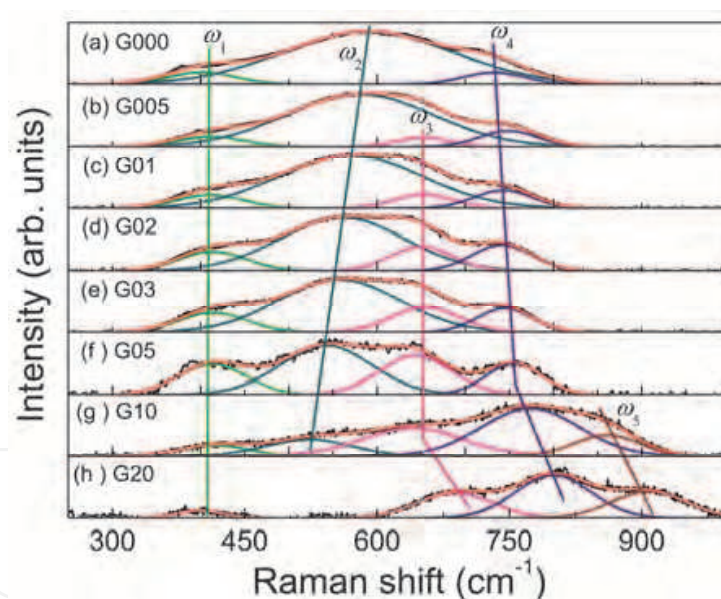
Fig. 9. The the typical spectrum of MgB_2 consisting of three broad peaks

The tensile strain was unambiguously detected in graphene-MgB_2 alloys made by diffusion process and the π energy gap was broadening with the graphene addition. The bond-stretching E_{2g} phonon mode splits into one soften mode due to the tensile strain and another harden mode due to the carbon substitution on boron sites. Although E_{2g} mode splitting have been observed in C doped MgB_2, both the two peaks shift to higher frequency and this is the first time to observe the coexistence of two modes shifting to opposite directions. The T_c value does not show enhancement because of impurity scattering effects and carbon substitution. However, higher T_c values are expected in graphene-MgB_2 alloys processed by proper techniques or made of stabilized graphene.

2.3.4 Upper critical field and irreversibility field

Figure 10 shows the upper critical field, H_{c2}, and the irreversibility field, H_{irr}, versus the normalised T_c for all the samples. It is noted that both H_{c2} and H_{irr} are increased by graphene doping. The mechanism for enhancement of J_c, H_{irr}, and H_{c2} by carbon containing dopants has been well studied. The C can enter the MgB$_2$ structure by substituting into B sites, and thus J_c and H_{c2} are significantly enhanced due to the increased impurity scattering in the two-band MgB$_2$ (Gurevich, A.,2003). Above all, C substitution induces highly localised fluctuations in the structure and T_c, which have also been seen to be responsible for the enhancements in J_c, H_{irr}, and H_{c2} by SiC doping.
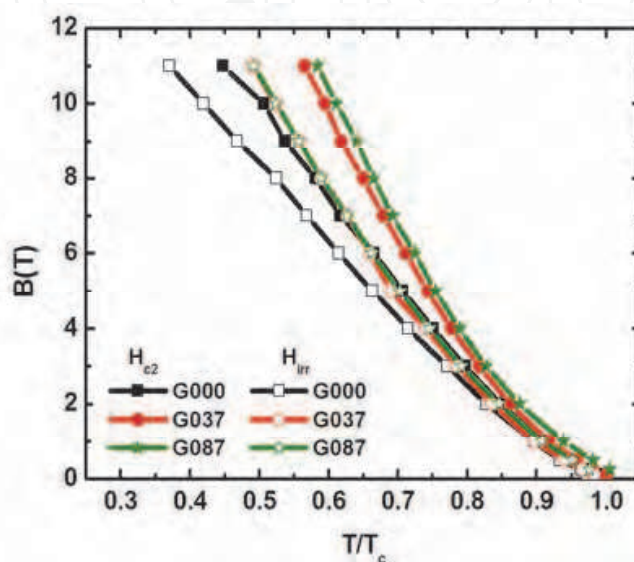

Fig. 10. Upper critical field, H_{c2}, and irreversibility field, H_{irr}, versus normalised transition temperature, T_c, for all graphenedoped and undoped MgB$_2$ samples (Xu, X. et al., 2010).

Furthermore, residual thermal strain in the MgB$_2$-dopant composites can also contribute to the improvement in flux pinning (Zeng, R. et al. 2009). In the present work, the C substitution for B (up to 3.7 at.%) graphene doping is lower, from the table 1, the change of the a-parameter is smaller, according to Avdeev et al result (Avdeev, M. et al., 2003), the level of C substitution, x in the formula Mg(B$_{1-x}$C$_x$) , can be estimated as x=7.5 × Δ(c/a), where Δ(c/a) is the change in c/a compared to a pure sample. As both the a-axis and the c-axis lattice parameters determined from the XRD data showed little change within this doping range the level of carbon substitution is low at this doping level. This is in good agreement with the small reduction in T_c over this doping regime. At 8.7 at% doping, there is a noticeable drop in the a-axis parameter, suggesting C substitution for B, which is also consistent with the reduction in T_c. The source of C could be the edges of the graphene sheets, although the graphene is very stable at the sintering temperature (850°C), as there have been reports of graphene formation on substrates at temperatures ranging from 870-1320°C (Coraux, J. et al., 2009). The significant enhancement in J_c and H_{irr} for G037 can not be explained by C substitution only.

2.3.5 Microstructure by TEM

The microstructure revealed by high resolution transmission electron microscope (TEM) observations show that G037 sample has grain size of 100-200 nm which is consistent with

value of the calculated grain size in table 1. The graphene doped samples have relatively higher density of defects compared with the undoped sample as shown in the TEM images of figure 11(a) and (c). The density of such defects is estimated to be 1/3 areas of TEM images, indicating high density in the doped samples. In figures 11(b) it should be noted that the order of fringes varies from grain to grain, indicates that the defect is due to highly anisotropic of the interface.
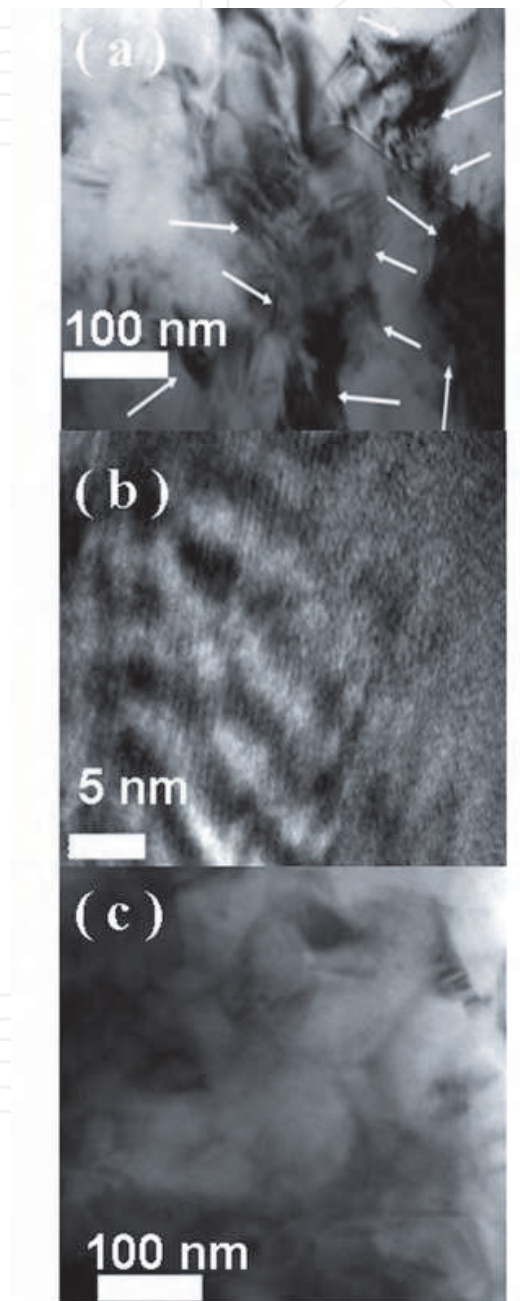

Fig. 11. (a) TEM image showing the defects with grains of the G037 sample with order of fringes varies between grains. Defects and fringes are indicated by arrow, and (b) HRTEM image of fringes. TEM images show large amount of defects and fringes can be observed in the graphene doped sample G037. (c) TEM image of the undoped sample for reference (Xu, X. et al., 2010).

Similar fringes have been reported in the MgB_2 (Zeng, R. et al. 2009), where these fringes were induced by tensile stress with dislocations and distortions which were commonly observed in the areas. As the graphene doped samples were sintered at 850°C for 10 hrs, the samples are expected to be relatively crystalline and contain few defects. Furthermore, as already shown above the C substitution level is low in graphene doped samples. Thus, the large amount of defects and amorphous phases on the nanoscale can be attributed to the residual thermal strain between the graphene and the MgB_2 after cooling because the thermal expansion coefficient of graphene is very small while that for MgB_2 is very large and highly anisotropic. The large thermal strain can create a large stress field, and hence structure defects and lattice distortion. These defects and distortions on the order of the coherence length, ξ, can play a role as effective pinning centres that are responsible for the enhanced flux pinning and J_c in the graphene doped MgB_2. The thermal strain-induced enhancement of flux pinning has also been observed in the SiC-MgB_2 composite as there is s noticeable difference in thermal expansion coefficient between MgB_2 and SiC (Coraux, J. et al., 2009).

3. Conclusion

In conclusion, the effects of graphene doping on the lattice parameters, T_c, J_c, and flux pinning in MgB_2 were investigated over a range of doping levels. By controlling the processing parameters, an optimised $J_c(B)$ performance is achieved at a doping level of 3.7 at.%. Under these conditions, J_c was enhanced by an order of magnitude at 8 T and 5 K while T_c was only slightly decreased. The strong enhancement in the flux pinning is argued to be attributable to a combination of C substitution for B and thermal strain-induced defects. Also, the evidence from collective pinning model suggests the δT_c pinning mechanism rather than the δl pinning for the graphene doped MgB_2, contrary to most doped MgB_2. The strong enhancement of J_c, H_{c2}, and H_{irr} with low levels of graphene doping is promising for large-scale MgB_2 wire applications.

Tensile strain effects on superconducting transition temperature (T_c) was observed in graphene-MgB_2 alloys to pursue high T_c in multi-gap superconductors. The enhancement of energy gap for π-band indicates the weak rescale of density of state on Fermi surface. The E_{2g} mode split into two parts: one dominant soften mode responding to tensile strain and another harden mode responding to carbon substitution effects. The existence of soften E_{2g} mode in bulk samples suggests that modified graphene-MgB_2 alloys are the potential candidates for the high performance superconducting devices.

The effects of graphene doping in MgB_2/Fe wires were also investigated. At 4.2K and 10T, the transport J_c was estimated to be for the wire sintered at 800°C for 30 minutes, the doped sample is almost improved as one order, compared with the best un-doped wire sample. The strong enchantment of the temperature dependence of the upper critical field (H_{c2}) and the irreversibility field (H_{irr}) is found from the resistance (R) – temperature (T). But the calculated active cross-sectional area fraction (A_F) represents the connectivity factor between adjacent grains is lower, which is the main factor to improve transport J_c in limitation. It should mention that in recently research activity, two groups can improve the mass density and the grain connectivity very well. One is the internal Mg diffusion processed (IMD) multi-filamentary wire, which is developed by Togano (Hur, J. M. et al., 2008). The other one is the cold high pressure densification (CHPD) in-situ MgB_2 wire by Flukiger [18]. If can

combine these methods with the graphene doping, the strong enhancement of J_c, H_{c2}, and H_{irr} with low levels of graphene doping is promising for large-scale MgB_2 wire in industrial applications.

4. Acknowledgment

5. References

Novoselov, K. S. et al. (2004). Electric field effect in atomically thin carbon films. *Science*, Vol.306, pp. 666–669, ISSN 0036-8075

Stankovich, S. et al. (2006). Graphene-based composite materials. *Nature*, Vol. 442, pp. 282–286, ISSN 0028-0836

Dou, S. X. et al. (2007). Mechanism of enhancement of electromagnetic properties of MgB_2 by nano-SiC doping. *Phys. Rev. Lett.*, Vol 98, pp. 097002-1, ISSN 0031-9007

Ma, Y. *et al*. (2006). Significantly enhanced critical current densities in MgB_2 tapes made by a scalable nanocarbon addition route. *Appl. Phys. Lett.*, Vol 88, pp. 072502-5, ISSN 0003-6951

Senlowocz, B. J. et al. (2005). Improved upper critical field in bulk-form magnesium diboride by mechanical alloying with carbon. *Appl. Phys. Lett.*, Vol 86, pp. 202502-5, ISSN 0003-6951

Kumakura, H. et al. (2004). Upper critical fields of powder-in-tube-processed MgB_2/Fe tape conductors. *Appl. Phys. Lett.*, Vol 84, pp. 3669-71, ISSN 0003-6951

Sumption, M. et al. (2005). Large upper critical field and irreversibility field in MgB_2 wires with SiC additions. *Appl. Phys. Lett.*, Vol 86, pp. 092507-10 ISSN 0003-6951

Dou, S. X. et al. (2003). Effect of carbon nanotube doping on critical current density of MgB_2 superconductor. *Appl. Phys. Lett.*, Vol 83, pp. 4996-9 ISSN 0003-6951

Kim, J. H. et al. (2006). Carbohydrate doping to enhance electromagnetic properties of MgB_2 superconductors. *Appl. Phys. Lett.*, Vol. 89, pp. 142505 -8 ISSN 0003-6951

Wilke, R. H. T. et al. (2008). Systematic effects of carbon doping on the superconducting properties of $Mg(B_{1-x}C_x)_2$. *Phys. Rev. Lett.*, Vol 92, pp. 062001 ISSN 0003-6951

Tung, V. C. et al. (2009). High-throughput solution processing of large-scale graphene. *Nature Nanotech.*, Vol 4, pp. 25-29, ISSN 1748-3387

Kim, K. S. et al. (2009). Large-scale pattern growth of graphene films for stretchable transparent electrodes. *Nature* , Vol 457, pp. 706-710, ISSN 0028-0836

Hernandez, Y. et al. (2008). High-yield production of graphene by liquid-phase exfoliation of graphite. *Nature Nanotech.* ,Vol 3, pp. 563–568, ISSN 1748-3387

Li, D. et al. (2008). Processable aqueous dispersions of graphene nanosheets. *Nature Nanotech.* ,Vol 3, pp. 101–105, ISSN 1748-3387

Li, X. et al. (2008). Chemically derived, ultrasmooth graphene nanoribbon semiconductors. *Science* Vol 319, pp. 1229–1232 ISSN 0036-8075

Choucair, M. Thordarson, P. and Stride, J. A. Gram-scale. (2009). Production of graphene based on solvothermal synthesis and sonication. *Nature Nanotech.* , Vol 4, pp. 30-33, ISSN 1748-3387

Nagamatsu, J. et al. (2001). Superconductivity at 39 K in magnesium diboride. *Nature*, Vol 410, No.6824, pp. 63-64, ISSN 0028-0836

Kunc, K. et al. (2001). MgB_2 under pressure: phonon calculations, Raman spectroscopy, and optical reflectance. *Journal of Physics -Condensed Matter*, Vol 13, No.44, pp. 9945-9962, ISSN 0953-8984

Soltanian, S. et al. (2005). High transport critical current density and large H_{c2} and H_{irr} in nanoscale SiC doped MgB_2 wires sintered at low temperature. *Superconductor Science & Technology*, Vol 18, No.5, pp. 658-666, ISSN 0953-2048

Yamamoto, A. et al. (2005). Universal relationship between crystallinity and irreversibility field of MgB_2. *Appl. Phys. Lett.*, Vol **86**, No.21 pp. 212502-5 ISSN 0003-6951

Dou, S. X. et al. (2002). Enhancement of the critical current density and flux pinning of MgB_2 superconductor by nanoparticle SiC doping. *Appl. Phys. Lett.*, Vol 81, No. 18, pp. 3419-3421, ISSN 0953-2048

Yeoh, W. K. et al. (2006). Control of nano carbon substitution for enhancing the critical current density in MgB_2. *Superconductor Science & Technology*, Vol 19, No.6, pp. 596-599, ISSN 0953-2048

Kim, J. H. et al. (2008). Correlation between doping induced disorder and superconducting properties in carbohydrate doped MgB_2. *Journal of Applied Physics*, Vol 104, No. 6, pp. 063911-6, ISSN 0021-8979

Dikin, D. A. et al. (2007). Preparation and characterization of graphene oxide paper. *Nature* Vol 448, pp. 457–460, ISSN 0028-0836

Xu, X. et al. (2010). Graphene doping to enhance the flux pinning and supercurrent carrying ability of a magnesium diboride auperconductor. *Superconductor Science & Technology*, Vol 23, pp. 085003-7, ISSN 0953-2048

Williamson, G. K., and Hall, W. H. (1953). X-ray line broadening from filed Aluminium and Wolfram. *Acta Metall*. Vol 1, pp. 22-31, ISSN 0001-6160

Horvat, J. et al. (2008). Transport and magnetic critical current in superconducting MgB_2 wires. *Superconductor Science & Technology*, Vol 21, pp. 065003-8, ISSN 0953-2048

Qin, M. J. (2002). Evidence for vortex pinning induced by fluctuations in the transition temperature of MgB_2 superconductors. *Phys. Rev. B.*, Vol 65, pp. 132508(4), ISSN 0163-1829

Wang, J. L. et al. (2008). Effects of C substitution on the pinning mechanism of MgB_2. *Phys Rev. B* Vol 77, pp. 174501(7), ISSN 0163-1829

Li, W. X. et al. (2008). Raman study of element doping effects on the superconductivity of MgB_2. *Phys. Rev. B.*, Vol 77, pp. 094517(9), ISSN 0163-1829

Gurevich, A. (2003). Enhancement of the upper critical field by nonmagnetic impurities in dirty two-gap superconductors. *Phys. Rev. B.*, Vol 67, pp.184515(7), ISSN 0163-1829

Zeng, R. et al. (2009). Thermal strain-induced enhancement of electromagnetic properties in SiC-MgB_2 composites. *Appl. Phys. Lett.*, Vol 94, 042510-3, ISSN 0003-6951

Avdeev, M. et al. (2003). Crystal chemistry of carbon-substituted MgB_2. *Physica C*, Vol 387 No.3-4, pp. 301-306. ISSN 0921-4534

Coraux, J. et al. (2009). Growth of graphene on Ir(111). *New J. Phys.,* Vol 11, pp. 023006-22. ISSN 1367-2630

Hur, J. M. et al. (2008). Fabrication of high-performance MgB$_2$ wires by an internal Mg diffusion process. *Superconductor Science & Technology*, Vol 21, pp. 032001-4, ISSN 0953-2048

Flukiger, R. Hossain, M. S. A. and Senatore, C. (2009) Strong enhancement of J_c and B_{irr} in binary *in situ* MgB$_2$ wires after cold high pressure densification. *Superconductor Science & Technology*, Vol 22, pp. 085002-8, ISSN 0953-2048

Rowell, J. M. (2003). The widely variable resistivity of MgB$_2$ samples. *Superconductor Science & Technology*, Vol 16, pp. R17-R27, ISSN 0953-2048
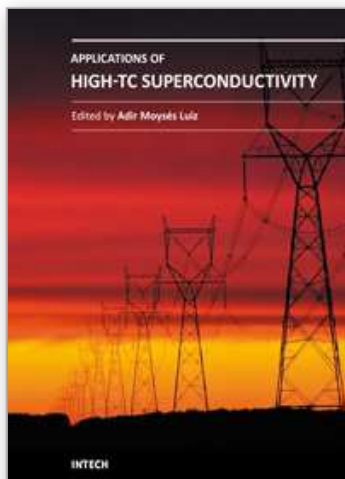
Applications of High-Tc Superconductivity

Edited by Dr. Adir Luiz

This book is a collection of the chapters intended to study only practical applications of HTS materials. You will find here a great number of research on actual applications of HTS as well as possible future applications of HTS. Depending on the strength of the applied magnetic field, applications of HTS may be divided in two groups: large scale applications (large magnetic fields) and small scale applications (small magnetic fields). 12 chapters in the book are fascinating studies about large scale applications as well as small scale applications of HTS. Some chapters are presenting interesting research on the synthesis of special materials that may be useful in practical applications of HTS. There are also research about properties of high-Tc superconductors and experimental research about HTS materials with potential applications. The future of practical applications of HTS materials is very exciting. I hope that this book will be useful in the research of new radical solutions for practical applications of HTS materials and that it will encourage further experimental research of HTS materials with potential technological applications.

How to reference

In order to correctly reference this scholarly work, feel free to copy and paste the following:

Xun Xu, Wenxian Li, Xiaolin Wang and Shi-Xue Dou (2011). Superconducting Properties of Graphene Doped Magnesium Diboride, Applications of High-Tc Superconductivity, Dr. Adir Luiz (Ed.), ISBN: 978-953-307-308-8, InTech, Available from: http://www.intechopen.com/books/applications-of-high-tc-superconductivity/superconducting-properties-of-graphene-doped-magnesium-diboride